A Band-Differenced Angular Signature Technique for Cirrus Cloud Detection

Larry Di Girolamo and Roger Davies

Abstract—A new approach to cloud detection is introduced that exploits the difference between two solar spectral reflectances as a function of view angle. The resulting *band-differenced angular signature* is sensitive to the contribution of Rayleigh scattering from above the tops of clouds and can be used to discriminate high clouds from lower level clouds and clear sky.

We use model simulations to show that this technique could be applied to measurements from the Multiangle Imaging SpectroRadiometer, scheduled for launch on the first platform of the Earth Observing System. Results show the technique to work best over ocean and snow surfaces. Over such surfaces, the minimum detectable high cloud optical thickness (at 0.55 μm) would typically be 0.5 without the use of any *a priori* scene information, and lower if such information is available.

I. INTRODUCTION

THE remote sensing of surface or atmospheric properties from satellites usually involves a common initial step—the partitioning of the data into either clear or cloudy pixels. There have traditionally been three typical approaches to this first step of cloud detection: radiance threshold techniques, radiative transfer model techniques, and statistical techniques [6], [12], [13]. Many variations within each approach exist, largely to cater to a particular data set with a particular task in mind, but all tend to share the common premise that the scene is to be classified using measurements of radiance from a single viewing direction. Here, we consider the additional advantages of using multidirectional information from the same scene.

Because past and present day satellite instruments have largely been single viewing or in the case of scanners, have tended to scan across the orbital track so that different view angles correspond to different scenes, the information content inherent to the anisotropy of the radiation field has yet to be exploited by remote sensing from space. Our study is nonetheless motivated by the prospect of measuring aspects of this anisotropy with a future instrument, the Multiangle Imaging SpectroRadiometer (MISR), which is scheduled for launch in 1998 on the first platform of the Earth Observing System [4].

This paper develops a new approach to remote sensing,

The authors are with the Department of Atmospheric and Oceanic Sciences, McGill University, Montreal, P.Q., Canada H3A 2K6.
IEEE Log Number 9402680.

which we call the *band-differenced angular signature* (or BDAS) technique, which assumes measurements of reflected solar radiation at two well-separated wavelengths are available from a given scene from a number of angles. While our approach is general, the subsequent discussion is oriented toward MISR measurements since these are likely to be the first to which the technique will be applied operationally. As shown below, the BDAS technique is well suited to the detection of thin high clouds, which frequently escape detection by traditional remote sensing techniques using reflected solar radiation. After first briefly summarizing the characteristics of the MISR instrument, we focus on the detectability of cirrus clouds over different surface types, and present model results to demonstrate the expected usefulness of the BDAS technique.

II. THE MULTIANGLE IMAGING SPECTRORADIOMETER

The Earth Observing System (EOS) is a program designed to carry out multidisciplinary earth science studies using a variety of remote sensing instruments that may share common satellite platforms [11]. One such instrument is the Multiangle Imaging SpectroRadiometer (MISR) [4], which will provide continuous multiangle coverage of the Earth at nine discrete angles, corresponding to viewing zenith angles at the surface of $0°$, $\pm26.1°$, $\pm45.6°$, $\pm60°$, and $\pm70.5°$. This is accomplished by four fixed cameras looking forward in the along-track direction, four looking aft, and one at nadir.

Each off-nadir camera is designed to give a similar cross-track resolution of ≈ 275 m, and to provide images in a push broom fashion in four spectral bands (443, 555, 670, and 865 nm) with a swath width of ≈ 360 km from an expected 705 km altitude sun-synchronous orbit. This will provide complete global coverage in times ranging from 2 d at the poles to 9 d at the equator. It will take ≈ 7 min in practice to view a given scene from $+70.5°$ to $-70.5°$, and we address the effect of such time dependence in Section III-D.

III. THE BAND-DIFFERENCED ANGULAR SIGNATURE TECHNIQUE

The BDAS approach first takes the difference in spectral reflectance between two well-separated wavelengths, and then examines this difference as a function of view

angle. As might be expected, the resulting signature is sensitive to the relative contribution of Rayleigh scattering to the total reflection. Since this contribution changes in the presence of clouds (e.g., [9]), especially high thick clouds, the resulting changes in the BDAS can allow such clouds to be readily detected.

To demonstrate the BDAS technique for a variety of situations, and to determine the limits of expected cloud detectability, we have examined many different simulations relevant to the MISR view angles and spectral channels. To maximize the spectral effect, we took the differences in the spectral reflectance at 0.44 and 0.86 μm. These differ by a factor of ≈ 15 in their sensitivity to Rayleigh scattering. The atmospheric model used was LOWTRAN 7 [8], which normally models the surface as a Lambertian reflector with a user-defined albedo. To include the other extreme of a specularly reflecting surface, we also replaced the LOWTRAN 7 surface by a flat ocean model surface that includes color, the details of which can be found in [3]. As shown below, however, the shape of the surface reflection function plays a small role when applying the BDAS technique. For this reason the Lambertian surface was retained for the examples of snow and land surfaces.

The Rayleigh scattering contribution to the BDAS increases rapidly as the cloud top is lowered in the atmosphere. As a result, it is much more difficult to distinguish low clouds from clear sky using the BDAS cloud detection criteria (given below) and detection of such clouds is better achieved by other conventional techniques. For this reason we have focused our attention on cirrus clouds—clouds that often pose difficulties to many detection algorithms. The cirrus model used was LOWTRAN 7's Cirrus cloud profile [8], [14], embedded in LOWTRAN 7's tropical atmosphere under light aerosol concentrations (Navy Maritime: 5 m/s wind speeds; air mass character = 1). The cirrus cloud was 1 km thick, and the cloud base height was varied between 4.5 km (corresponding to the model's 0°C isotherm) and 19 km (maximum observed height from [5]). The cloud optical thickness at a wavelength of 0.55 μm was also varied, and all viewing and solar geometries were examined.

A. Ocean BDAS

Fig. 1 shows the BDAS for clear and cloudy skies over different ocean surfaces, all at a solar zenith angle of 60° and a relative azimuth angle φ_r of 0° (i.e., viewing in the solar plane). The difference in the shape of the clear and cloudy BDAS is greatest at forward scattering angles (plotted as negative viewing angles). Here, the cloudy band-differenced reflectance increases towards nadir, whereas the clear band-differenced reflectance decreases. This characteristic is typical of most scenes. The BDAS shape depends on the sun and viewing geometry as well as cloud-top height, cloud optical thickness, and surface spectral albedo. As will become apparent from later figures, we generally find that the higher and thicker the
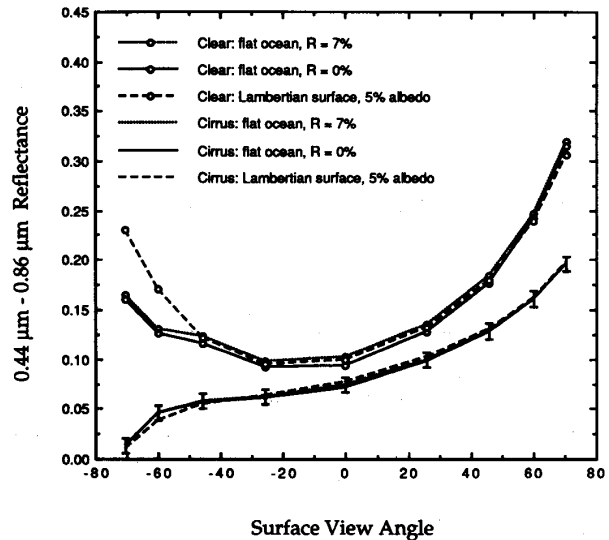

Surface View Angle

Fig. 1. Band-differenced angular signatures over different ocean surfaces for a solar zenith angle of 60° and $\varphi_r = 0°$. R is the ratio of up-welling to down-welling 0.44 μm irradiance just below ocean surface. $R = 7$ percent corresponds to clear ocean and $R = 0$ percent corresponds to yellow substance dominated ocean [15]. The cirrus cloud is 1 km thick with a base height of 5 km and a 0.55 μm optical thickness of 1.0. The error bars (due to estimated MISR measurement uncertainty) shown for the cirrus cloud over $R = 0$ percent ocean are typical in magnitude for the other curves.

cloud, the larger the slope of the BDAS in the forward viewing direction.

As shown in Fig. 1, the effect of ocean color is small. A comparison of a Lambertian surface of similar albedo to that of the flat ocean is also depicted. The difference in BDAS between the flat ocean model and the Lambertian surface is typically small, with exceptions occurring where the specular peak is encountered. This is also shown in Fig. 1, where the specular peak occurs at a view angle of −60°. In this direction, the band-differenced reflectance of the Lambertian surface model overestimates the band-differenced reflectance of the flat ocean model. Otherwise, the band-differenced angular signatures are very similar. In the cloudy case, the BDAS is very similar for both surfaces since the radiation field (both incoming and surface reflected) is much more diffuse in the presence of clouds. Thus, in two extreme surface scenarios it would appear that the BDAS is relatively insensitive to the surface reflection function, as long as the shape of the surface reflection function is similar at both 0.44 and 0.86 μm.

In order to measure the performance of the BDAS for cirrus cloud detection, this study also sought the minimum detectable cloud optical thickness (τ_m). Because the absolute value of the band-differenced reflectance depends on factors such as aerosol and water vapor concentrations, cloud optical thickness, surface albedo, and so forth, the cloud detection criterion must be based on the BDAS shape alone. In this way no *a priori* information about the scene is necessary. The cloud detection criterion for this study was simple: a high cloud was assumed pres-
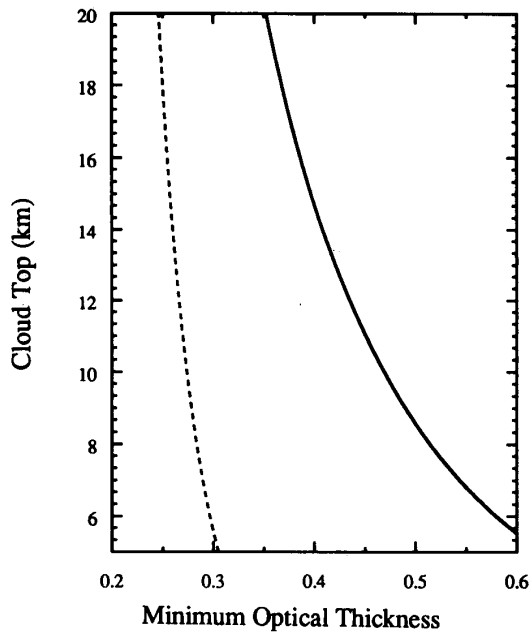
Fig. 2. Minimum detectable cirrus cloud 0.55 μm optical thickness (τ_m) as a function of cloud top height. The dashed line is for a solar zenith angle of 60° and $\varphi_r = 0°$. The solid line is for a solar zenith angle of 60° and $\varphi_r = 60°$.

ent if, within measurement uncertainty, the BDAS had a slope 0 for all viewing directions. The measurement uncertainty expected for MISR [1], [2] is included in Fig. 1.

Fig. 2 shows the minimum detectable cloud optical thickness as a function of height for two cases over a 5 percent Lambertian surface. The first is for a solar zenith angle of 60° and $\varphi_r = 0°$, while the second has $\varphi_r = 60°$. Note that the rate of increase in τ_m as the cloud is lowered is larger for larger φ_r. This is generally the case for all solar zenith angles and surface types.

The minimum detectable cloud optical thickness, 5 km base height, over ocean is shown in Fig. 3(a) (flat ocean model: 0.44 μm color = 0 percent) and (b) (Lambertian surface: 5 percent albedo; flat ocean model: 0.44 μm color = 7 percent). Note that they are nearly identical, confirming the general lack of sensitivity to the details of the ocean surface. The plots are polar, with the solar zenith angle given by the radius and φ_r given by the azimuth. Note the increase in τ_m with increasing φ_r. Excellent results are obtained for φ_r less than $\approx 45°$, for which an average value of $\tau_m \approx 0.5$ is obtained. At large solar zenith angles and small φ_r, the results improve to $\tau_m \approx 0.1$ and as φ_r approaches 90° they degrade to $\tau_m \approx 5$.

B. Snow BDAS

As discussed above, the shape of the surface reflection function plays a second-order role. For snow, the asymmetry parameter is nearly the same at 0.44 and 0.86 μm [21]. Hence, the shape of the reflection function at these wavelengths should also be similar. For this reason the

Lambertian surface model was used for snow. Three different snow surfaces, all taken from [20], were examined: pure snow, snow with 1 parts per million by weight (ppmw) of soot, and snow with 10 ppmw of soot. Figs. 3(c), (d), and (e) show τ_m over these surfaces. The darkened areas are where the cloud detection criterion fails. This is illustrated in Fig. 4, where the clear sky example for pure snow meets the classification criterion for a cirrus cloud. When this situation occurs, the location on the polar plot is flagged as a failure and is shaded black. For the other surfaces shown in Fig. 4, the cloud detection criterion is met.

There are several interesting features in the snow surface results of Fig. 3. First, note that the shaded regions occur at small solar zenith angles. This is not a problem for polar locations since the sun does not reach such small zenith angles. Snow-capped mountains, however, that are further equatorward, may not meet the detection criterion. The good sensitivity to cloud presence is also noted. What may seem strange at first is the abrupt transition from nondetection (shaded region) to detection with a high sensitivity to cloud presence ($\tau_m \approx 0.1$). This can be explained by considering the BDAS of the snow surface with 1 ppmw soot in Fig. 4. This clear sky BDAS lies on the edge of detectability in terms of the cloud detection criterion. Thus, only a thin cirrus cloud is required to sufficiently mask the clear sky signature for the cloud detection criterion to be met resulting in the sharp transition zone between nondetectability and high sensitivity to cirrus cloud presence. One last item to note is the region of poor detection at large solar zenith angles and large φ_r, as for the ocean case.

C. Land BDAS

The ideal Lambertian surface reflection model may not be appropriate for the BDAS simulation over land, because for many vegetated surfaces the shape of the reflection function from 0.44 to 0.86 μm may differ significantly [7]. Nonetheless, the Lambertian surface was still used as an approximation in calculating the BDAS. The 0.44 and 0.86 μm albedos were set at 0.05 and 0.40, respectively. Fig. 5 gives an example of a BDAS over land while Fig. 3 (f) gives the plot for τ_m. Fig. 3 (f) indicates that the BDAS technique would work poorly over land surfaces except for large solar zenith angles and small φ_r. The poor cloud detectability over land using the BDAS is attributed to the large difference in reflectance from 0.44 and 0.86 μm.

D. Other Factors

The main remaining factors that may at times affect the BDAS and the detection of cirrus clouds include the effects of water vapor, tropospheric and stratospheric aerosols, ice crystal habit, and misregistration. Of these, tropospheric aerosols typically occur at low enough altitudes that they should generally have a negligible effect on the shape of the BDAS and a very small effect on its magni-
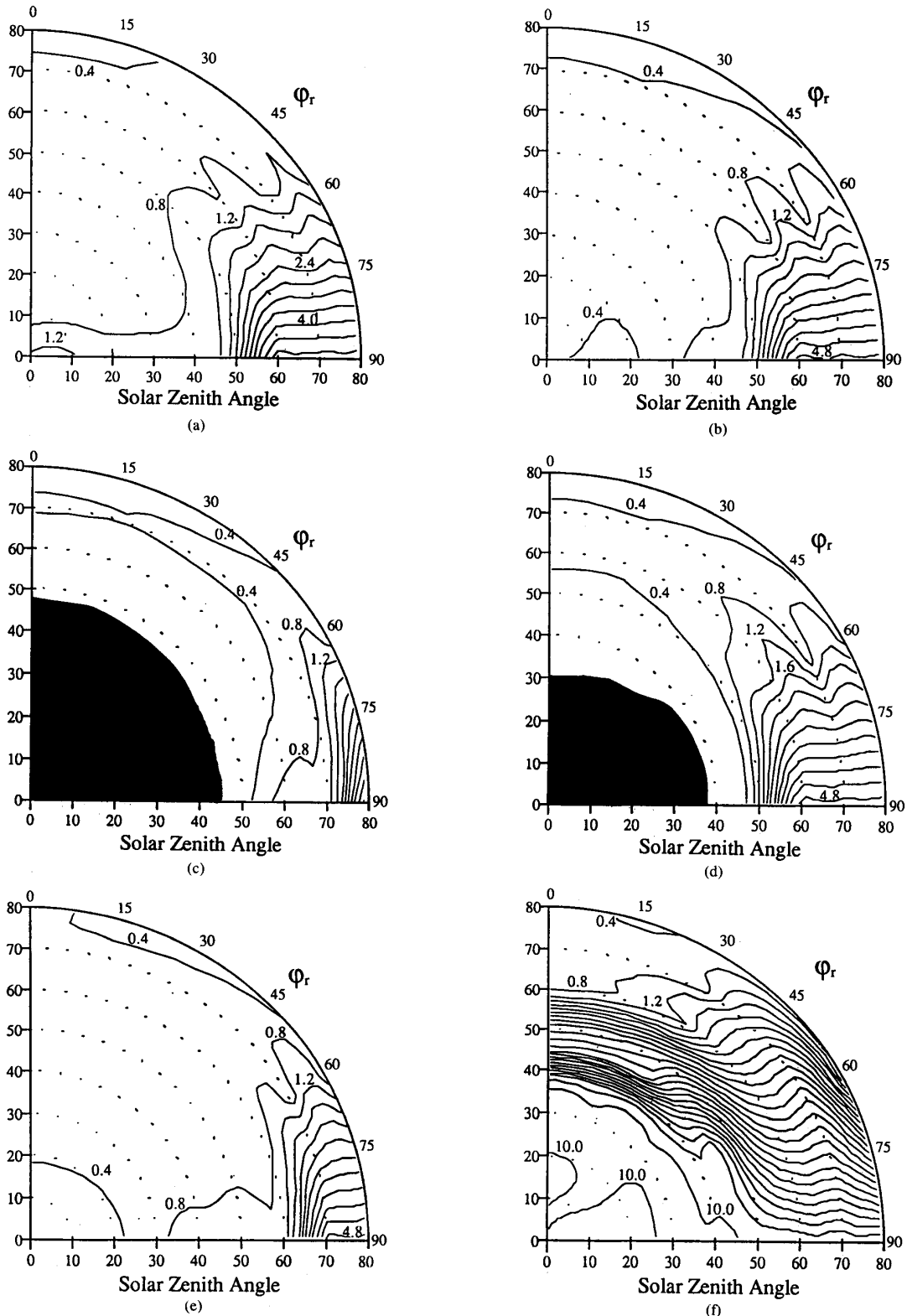
Fig. 3. Minimum detectable cirrus cloud 0.55 μm optical thickness (τ_m) for a (a) $R = 0$ percent ocean surface, (b) $R = 7$ percent ocean surface with the 5 percent Lambertian surface having the same results, (c) pure snow surface, (d) pure snow surface with 1 ppmw soot, (e) pure snow surface with 10 ppmw soot, and (f) typical land surface. Cloud base height = 5 km.
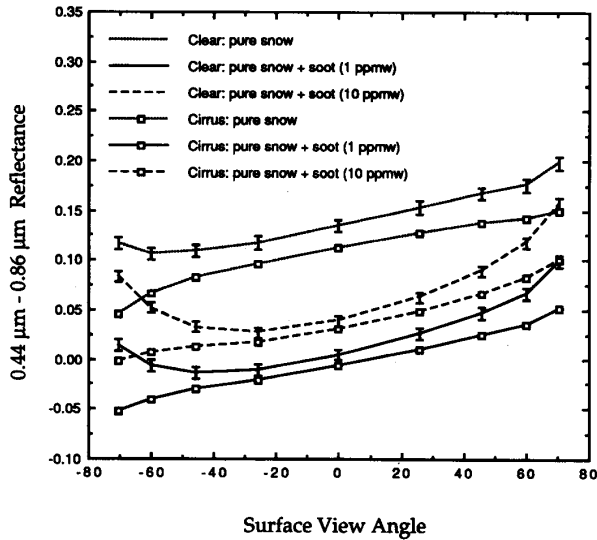
Fig. 4. Band-difference angular signatures over snow for a solar zenith angle of 45° and $\varphi_r = 0°$. The cirrus cloud is 1 km thick with a base height of 5 km and a 0.55 μm optical thickness of 0.5. The error bars (due to estimated MISR measurement uncertainty) denoted on the clear sky curves are similar for the corresponding cirrus curves.
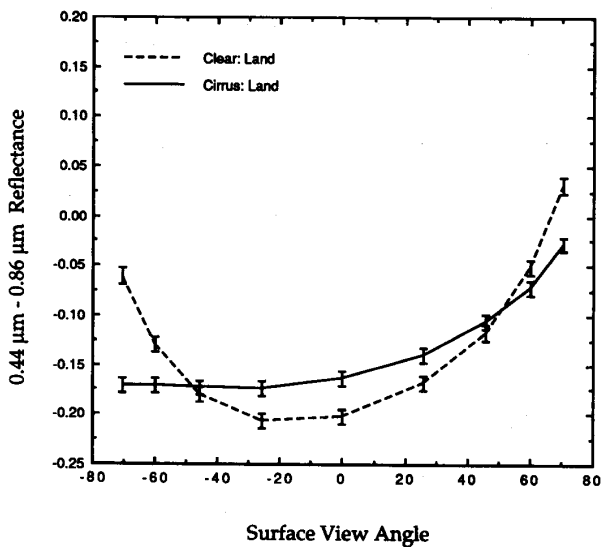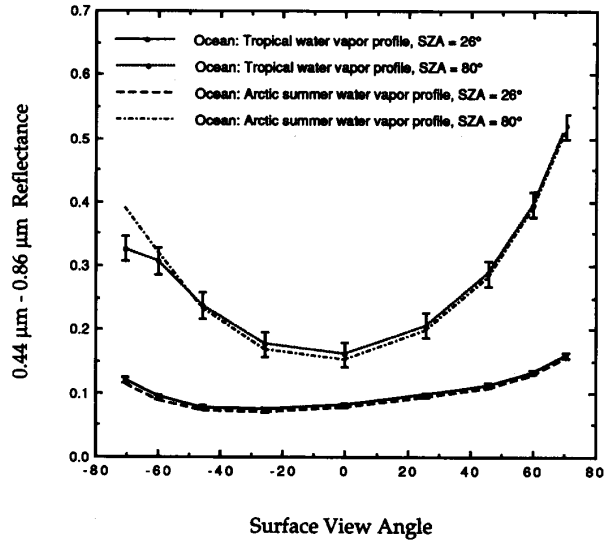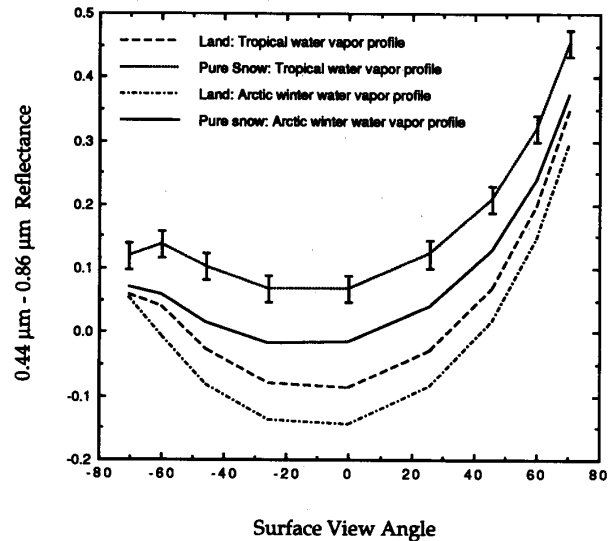

Surface View Angle

Fig. 5. Band-differenced angular signatures over a typical land surface for a solar zenith angle of 60° and $\varphi_r = 30°$. The cirrus cloud is 1 km thick with a base height of 5 km and a 0.55 μm optical thickness of 1.0. Error bars are calculated using estimates of MISR measurement uncertainty.

Surface View Angle

(a)

Surface View Angle

(b)

Fig. 6. Clear sky band-differenced angular signature showing the effects of water vapor over (a) ocean surface for different solar zenith angles (SZA) with $\varphi_r = 0°$, and (b) snow and land surfaces for a solar zenith angle of 80° with $\varphi_r = 0°$. The error bars (due to estimated MISR measurement uncertainty) for (a) are similar for the curves having the same solar zenith angle, and (b) are similar for all curves.

tude. A larger effect may be attributed to water vapor variability, since extinction at 0.86 μm can be comparable to molecular scattering for high water vapor amounts. To assess its effect on the BDAS, a comparison is shown in Fig. 6 using water vapor profiles for tropical and subarctic winter atmospheres [8], keeping all other meteorological parameters constant. Fig. 6(a) shows the water vapor effect is indeed negligible over an ocean surface, and Fig. 6(b) shows that over land or snow, while there is a dif-

ference in the magnitude of the BDAS, its shape is relatively unaffected. The effect of water vapor on τ_m is thus small and does not change the results presented in Fig. 3.

The effect of ice crystal habit was also investigated. From the results of Takano and Liou [17], [18], the difference between the reflection function at 0.86 μm and that at 0.44 μm is practically the same for cirrus clouds composed of spherical or hexagonal crystals. The BDAS is therefore insensitive to assumptions about crystal habit, whereas the cloud reflection function itself may depend

significantly on crystal habit. By extension, the BDAS technique should work in nonplane-parallel cloudy situations as long as the reflection function remains the same from 0.86 to 0.44 μm.

Stratospheric aerosol can at times pose a greater problem. Following the eruption of Mt. Pinatubo, for example, optical depths up to 0.4 (at 0.5 μm) were reported by Valero and Pilewskie [19]. Layers as thick as this would give similar, but not identical, band-differenced angular signatures. While the differences in signature can likely be exploited to identify such special cases, the details of this are left for future study.

Finally, the possibility of pixel misregistration is a problem that potentially affects the practical implementation of the BDAS technique. Given the expected pointing and navigational accuracy of forthcoming satellite systems, the main source of misregistration in the present context is due to the effect of cloud displacement during the time it takes measurements to be made from different directions. For example, in the 3.5 min that elapse between measurements of a given location from nadir and the most oblique view by MISR, a cloud field may be advected several kilometers. If the cloud field is horizontally uniform over such distance, this is of little consequence; but in general, a correction based on the assumed wind field should first be made, as will be characteristic of all cloud remote sensing techniques using multiangle views. We also note, however, that the effect of pixel misregistration can be minimized in our context by calculating the slope of the BDAS successively for adjacent pairs of view angles, and by paying particular attention to the most oblique measurements in the forward scattering direction, since this is where most of the BDAS signal for cirrus detection resides.

IV. CONCLUSION

We have shown the potential use of satellite-based angular radiometric measurements for cirrus cloud detection. A new technique, namely band-differenced angular signature (BDAS), uses measurements of spectral solar radiances at a number of angles from the same scene, and prospects of obtaining such measurements come from the EOS/MISR. We have modeled the BDAS for a number of scenes involving thin cirrus. The BDAS technique performs best at cloud detection over ocean and, interestingly, over snow surfaces where most other satellite cloud detection algorithms experience difficulties. The minimum detectable cloud optical thickness (τ_m) was typically about 0.5 without the use of any a priori scene information. With a priori scene information, interpretation of the BDAS can be further improved to yield smaller τ_m. Moreover, this study has only addressed the initial step of any scene analysis—that of cloud detection. Further information about the cloud, for example, may be possible through both shape and magnitude of the BDAS.

Over land, without a priori information, reasonable results ($\tau_m \approx 0.5$) are obtained only for large solar zenith

angles and small φ_r. At other angles over land, knowledge of the potentially large difference in surface reflectance from 0.44 and 0.86 μm will be required (a priori) in order to exploit the BDAS for cloud detection. However, the BDAS technique may still find application in multilayered cloud systems over land. For example, a simple reflectance thresholding technique may detect a low, thick stratiform cloud but not an overlying thin cirrus cloud. When low clouds mask much of the spectral difference of land surface reflectances (e.g., [16]), the BDAS technique should then be able to detect overlying thin cirrus cloud.

A comparison of the BDAS technique with other cloud detection techniques can only be made qualitatively. The performance of any cloud detection technique depends on the data set to which it is applied. Most techniques also require other additional scene information (e.g., temperature and humidity profiles), which may not be available. The availability and quality of such a priori information will affect the cloud detection performance. Nonetheless, reports of moderate resolution satellite-sensor have detected cloud optical thickness as low as 0.2 (e.g., [10]) with the use of a priori scene information. We note that the BDAS technique should frequently perform this well (depending on surface type, cloud height, and sun-view geometry) without the use of a priori scene information.

It should also be noted the BDAS technique is, thus far, academic; this is the first study that explores the possibility of using angular signatures for the purpose of cloud detection. Use of angular signatures in cloud analysis is in its infancy, as was the use of spectral signatures in the early 1960's. Once multiangle data sets become routinely available, the relative potential of angular signatures, and of the BDAS technique in particular, will be evaluated on a practical basis.

REFERENCES

[1] N. C. L. Chrien, C. J. Bruegge, and B. R. Barkstrom, "Estimation of calibration uncertainties for MISR via fidelity intervals," SPIE, vol. 1939, Sensor for the early Earth Observing Syst. platforms, April, 13, pp. 114–125, 1993.

[2] N. C. L. Chrien, "Fidelity intervals," Jet Propulsion Lab., MISR Design File Memor. 82, February 25, 1992.

[3] L. Di Girolamo, "On the detection of cirrus clouds from satellite measurements," Centre for climate and global change research, M.Sc. thesis, McGill University, Montreal, Canada, Rep. 92-8, 1992.

[4] D. J. Diner, J. V. Bruegge, J. V. Martonchik, T. P. Ackerman, R. Davies, S. A. W. Gerstl, H. R. Gordon, P. J. Sellers, J. Clark, J. A. Daniels, E. D. Danielson, V. G. Duval, K. P. Klaasen, G. W. Lilienthal, D. I. Nakamonto, R. J. Pagano, and T. H. Reilly, "MISR: A Multiangle Imaging SpectroRadiometer for geophysical and climatological research for EOS," IEEE Trans. Geosci. Remote Sens., vol. 27, pp. 200–214, 1989.

[5] D. R. Dowling and L. F. Radke, "A summary of the physical properties of cirrus clouds," J. Appl. Meteorol., vol. 29, pp. 970–978, 1990.

[6] A. H. Goodman and A. Henderson-Sellers, "Cloud detection analysis: A review of recent progress," Atmos. Res., vol. 21, pp. 203–228, 1988.

[7] D. S. Kimes, W. W. Newcomb, R. E. Nelson, and J. B. Schutt, "Directional reflectance distributions of a hardwood and pine forest canopy," IEEE Trans. Geosci. Remote Sens., vol. GE-24, pp. 281–293, Mar. 1986.

[8] F. X. Kneizys, E. P. Shettle, L. W. Abreu, J. H. Chetwynd, G. P.

Anderson, W. O. Gallery, J. E. A. Selby, and S. A. Clough, "User's guide to LOWTRAN 7,"AFGL-TR-88-0177, 1988.

[9] Y. Mekler and M. Podolak, "Estimation of cloud top heights from satellite imagery," *Appl. Opt.*, vol. 24, pp. 2419-2422, 1985.

[10] P. Minnis, D. F. Young, K. Sassen, J. M. Alvarez, and C. J. Grund, "The 27-28 October 1986 FIRE IFO cirrus case study: Cirrus parameter relationships derived from satellite and lidar data," *Mon. Weath. Rev.*, vol. 118, pp. 2402-2425, 1990.

[11] "Earth observing system, science and mission requirements working group report and appendix," vol. 1, NASA, TM-86129, 1984.

[12] W. B. Rossow, F. Mosher, E. Kinsella, A. Arking, M. Desbois, E. Harrison, P. Minnis, E. Ruprecht, G. Seze, C. Simmer, and E. Smith, "ISCCP cloud algorithm intercomparison," *J. Clim Appl. Meteorol.*, vol. 24, pp. 877-903, 1985.

[13] W. B. Rossow, "Measuring cloud properties from space: A review," *J. Clim.*, vol. 2, pp. 201-213, 1989.

[14] E. P. Shettle, F. X. Kneizys, S. A. Clough, G. P. Anderson, L. W. Abreu, and J. H. Chetwynd, "Cloud models in LOWTRAN and FASCODE," in *Proc. CIDOS-88*, Oct. 18-20, 1988, Silver Springs, MD.

[15] S. Sathyendranath and A. Morel, "Light emerging from the sea—Interpretation and uses in remote sensing," in *Remote Sensing Applications in Marine Science and Technology*, A. P. Cracknell, Ed., NATO ASI Series, 1983, pp. 323-357, Dordrecht, Holland.

[16] R. W. Saunders and K. T. Kriebel, "An improved method for detecting clear sky and cloudy radiances from AVHRR data," *Int. J. Remote Sens.*, vol. 9, pp. 123-150, 1988.

[17] Y. Takano and K. M. Liou, "Solar radiative transfer in cirrus clouds, Part I: Single-scattering and optical properties of hexagonal ice crystals," *J. Atmos. Sci.*, vol. 46, pp. 3-19, 1989.

[18] ——, "Solar radiative transfer in cirrus clouds, Part II: Theory and computation of multiple scattering in an anisotropic medium," *J. Atmos. Sci.*, vol. 46, pp. 20-36, 1989.

[19] F. P. J. Valero and P. Pilewskie, "Latitudinal survey of spectral optical depths of the Pinatubo volcanic cloud—derived particle sizes, columnar mass loadings, and effects on planetary albedo," *Geophys. Res. Lett.*, vol. 19, no. 2, pp. 163-166, 1992.

[20] S. G. Warren and W. J. Wiscombe, "A model for the spectal albedo of snow, II. Snow containing atmospheric aerosols," *J. Atmos. Sci.*, vol. 37, pp. 2734-2745, 1980.

[21] W. J. Wiscombe and S. G. Warren, " A model for the spectral albedo of snow, I. Pure snow," *J. Atmos. Sci.*, vol. 37, pp. 2712-2733, 1980.

Larry Di Girolamo received the B.Sc.(Hons.) degree in astrophysics from Queen's University at Kingston, Kingston, Ont., Canada, in 1989, and the M.Sc. degree in meteorology from McGill University, Montreal, P.Q., Canada, in 1992.

He is currently a National Science and Engineering Research Council of Canada Scholar at McGill University working toward the Ph.D. degree under the supervision of Professor R. Davies. His present research is focused on the development of remote sensing techniques for the upcoming Multiangle imaging spectroradiometer (MISR)—part of the EOS-NASA AM-platform.

Roger Davies was born in London, England, and educated in England, Scotland, New Zealand, and the United States. He received the B.Sc.(Hons.) degree in physics from Victoria University, Wellington, NZ in 1970 and the Ph.D. degree in meteorology from the University of Wisconsin-Madison in 1976.

Currently, he is an Associate Professor with the Department of Atmospheric and Oceanic Sciences at McGill University, Montreal, P.Q., Canada, where he teaches courses on climate theory and remote sensing. His research interests are mainly in atmospheric radiation, especially three-dimensional radiative transfer and the interaction c f clouds with radiation.

Dr. Davies is a member of the MISR science team, a member of the International Radiation Commission, and a member of the Joint Working Group on Clouds and Radiation of the International Association of Meteorology and Atmospheric Physics.